
Article:
Gao, H., Chen, J., Liu, W. orcid.org/0000-0003-2968-2888 et al. (2 more authors) (2020) Phase inconsistency error compensation for multichannel spaceborne SAR based on the rotation-invariant property. IEEE Geoscience and Remote Sensing Letters. ISSN 1545-598X

https://doi.org/10.1109/lgrs.2020.2972402

Phase Inconsistency Error Compensation for Multi-channel Spaceborne SAR Based on the Rotation-Invariant Property

Heli Gao, *Student Member, IEEE,* Jie Chen, *Senior Member, IEEE,* Wei Liu, *Senior Member, IEEE,* Chunsheng Li, and Wei Yang, *Member, IEEE*

***Abstract*—The azimuth multi-channel technique has been widely used in synthetic aperture radar (SAR) systems for improving the resolution and expanding the illumination area. However, due to phase inconsistency of different channels, the image quality deteriorates significantly, including resolution loss and appearance of ghost targets. In this work, by exploiting the rotation-invariant property of the steering vector of the multi-channel SAR signal, a phase inconsistency error compensation method is proposed based on the estimation of signal parameters by rotation invariance technique (ESPRIT). Experimental results are presented using both simulated and real data to demonstrate the performance of the proposed method.**

***Index Terms*—multi-channel, phase inconsistency, synthetic aperture radar (SAR), estimation of signal parameters by rotation invariance technique (ESPRIT).**

I. Introduction

HIGH azimuth resolution and wide-swath imaging present conflicting demands on synthetic aperture radar (SAR) system design. In order to acquire a wide illumination area in range, low pulse repetition frequency (PRF) has to be adopted in the single-channel SAR system, which inevitably limits the azimuth processing bandwidth and results in azimuth resolution loss. Multi-channel SAR systems can effectively alleviate this problem by adding the azimuth receiving channel [1], [2], which means more sampling points can be obtained in the low PRF case. Nowadays, multi-channel technology has been verified by Radarsat-2 [3] and TerraSAR-X [4] and is planned for future advanced SAR systems. Corresponding processing algorithms for multi-channel SAR have been discussed by many researchers [1], [5]. However, there exist channel inconsistency errors among azimuth receiving channels due to various environmental factors, such as temperature fluctuation and electromagnetic radiation, which will degrade the ultimate image results, including loss of azimuth resolution and appearance of ghost targets.

The channel inconsistency errors are composed of amplitude, phase, timing delay and equivalent phase center position errors. The amplitude inconsistency errors can be corrected by channel balancing [6] and timing delay errors can be estimated using azimuth cross-correlation [7]. The along-tracking position inconsistency errors can be neglected while position inconsistency errors in line of sight can be integrated into the phase inconsistency (PI) errors [8]. To tackle the challenge caused by PI errors, several methods were proposed in literature. The Multiple Signal Classification (MUSIC) technique was introduced for estimation of PI errors in [9], which treats clutter spectrum components as the known "virtual" calibration sources. Based on MUSIC technology, orthogonal subspace (OS) method [9], signal subspace comparison (SSC) method [6], and conjugation method [10] (collectively referred to as MUSIC methods) were proposed by constructing several different cost functions. Unfortunately, the signal-to-noise-ratio (SNR) is not considered in these methods. In order to improve estimation accuracy, an adaptively weighted least squares (AWLS) algorithm was proposed [11], which is based on minimizing the impact on the spectrum outside main bandwidth caused by PI errors. Although SNR is involved in this method, its performance degrades significantly in the case of near coincidental sampling [12], which means high sampling non-uniformity. Another drawback of MUSIC methods and the AMLS method is that the available Doppler bins for estimation may be insufficient when the equivalent PRF is only a little larger than the 3dB bandwidth of the signal. Similarly, a Doppler spectrum optimization (DSO) algorithm which aims to maximize the spectrum power in main bandwidth is proposed in [13]. Although it can employ enough Doppler bins as calibration sources, it still faces the challenge of coincidental sampling, and is time-consuming due to the iterative processing. Moreover, the above mentioned methods need an accurate Doppler centroid estimator to select suitable Doppler bins as calibration sources, which may not be practical in multi-channel SAR due to Doppler ambiguity. The spatial cross-correlation coefficient (SCCC) method based on azimuth interferometry was introduced [7], which incorporates Doppler centroid estimation in its procedure. However, its estimation accuracy is worse than other methods for inhomogeneous scenes, which limits its application.

There are mainly four factors to be considered for an estimation method for PI errors, including accuracy against SNR, robustness against uniformity, computational efficiency

Manuscript received X xx, 2019; revised X xx, 2019 and X xx, 2019; accepted X xx, 2019. Date of publication X xx, 2019; date of current version X xx, 2019. This work is supported by the National Natural Science Foundation of China (NSFC) under Grant No. 61861136008 and Grant No. 61701012 and Fundamental Research Funds for the Central Universities under Grand No. YWF-19-BJ-J-304.

Heli Gao, Jie Chen, Chunsheng Li and Wei Yang are with the School of Electronic and Information Engineering, BeiHang University, Beijing 100191, China (e-mail: gaohl@buaa.edu.cn; chenjie@buaa.edu.cn; lics@buaa.edu.cn; yangweigigi@sina.com). Chunsheng Li is also with Collaborative Innovation Center for Geospatial Information Technology, Wuhan, China. Wei Liu is with the Department of Electronic and Electrical Engineering, University of Sheffield, Sheffield, S10 2TN, United Kingdom (e-mail: w.liu@sheffield.ac.uk).

Color versions of one or more of the figures in this letter are available online at http://ieeexplore.ieee.org.

Digital Object Identifier x.x/xxx

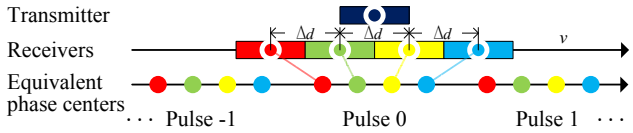

Fig. 1: Effective mode of multi-channel SAR in azimuth.

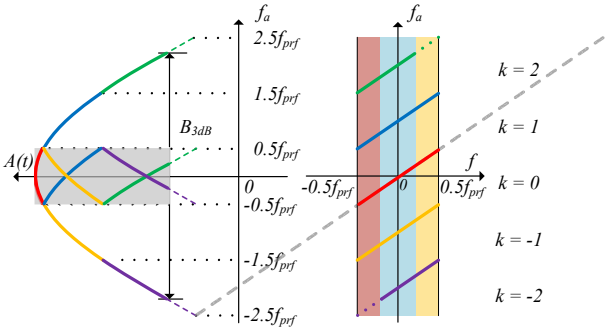

Fig. 2: Doppler spectrum of multi-channel SAR and index of ambiguity spectrum segments. $A(t)$ and f_a represent the spectrum amplitude and Doppler frequency, respectively. The curved segments in the grey shadow are the aliased spectrums of multi-channel SAR. The subfigure at right represents the relationship between Doppler frequency and baseband frequency. The three colored backgrounds (pink, blue and gold) indicate the spectrums with different ambiguity indexes.

and ability to estimate Doppler centroid. Considering these factors, in this paper, a novel PI error estimation method based on the ESPRIT [14] is proposed. First, the rotation invariance property of the steering vector of the multi-channel SAR signal in one Doppler bin is derived. By this property, eigenvalues of the spectrum matrix of multi-channel signals are uniformly distributed in the ideal case. In the case with PI errors, by contrast, the distribution of these eigenvalues is non-uniform. Therefore, the PI errors can be estimated by minimizing this kind of difference. In order to solve the cross-interference between the eigenvalues, a quick estimation strategy is introduced, and the Doppler centroid estimation can be conveniently incorporated into this strategy.

This letter is organized as follows. The data model for a multi-channel SAR is reviewed in Section II and its rotation invariance property is analyzed in Section III. The proposed ESPRIT based estimation method is proposed in Section IV. In Section V, simulation results are provided to show the effectiveness of the proposed method in comparison with exiting methods. Conclusions are drawn in Section VI.

II. Model of Multi-Channel SAR Signal

Generally, the transmitter and receivers are separated in a multi-channel SAR system (see Fig. 1). Subject to phase compensation [2], it is equivalent to a mono-static SAR whose phase centers are virtually located at the midpoint between transmitter and receivers. The multi-channel SAR signal can be considered as a replica of the reference single-channel SAR signal with a delay. Assuming M is the number of azimuth channels, the signal received by the m-th channel of a multi-channel SAR system can be expressed as

$$s^{(m)}(\tau,t)=u(\tau,M\cdot t-\Delta t_m),1\le m\le M, \tag{1}$$

in which τ is the range fast time, t is the azimuth slow time and $u(\tau,t)$ represents the reference single-channel SAR signal. Δt_m denotes the equivalent time delay, given as

$$\Delta t_m=\left(m-\frac{M+1}{2}\right)\Delta t,\ \ \Delta t=\frac{\Delta d}{2v}, \tag{2}$$

where v is the velocity of the SAR sensor, Δt and Δd are the along-track equivalent time delay and displacement interval of adjacent channels, respectively. Since the Doppler bandwidth is larger than PRF in each channel, the spectrum after applying the Fast Fourier Transform (FFT) is aliased as

$$S^{(m)}(\tau,f)=\mathrm{e}^{j\delta_m}\sum_k U(\tau,f+k\cdot f_{prf})\,e^{j2\pi(f+k\cdot f_{prf})\Delta t_m} \tag{3}$$

where $U(\tau,f)$ is the spectrum of the single-channel strip-map SAR signal $u(\tau,t)$, δ_m is the PI error in the m-th channel, f is the baseband Doppler frequency, f_{prf} represents the pulse repetition frequency and k denotes the index of the ambiguity components at a certain Doppler gate with $k_1\le k\le k_2$. Note that k_1 and k_2 are the minimum and maximum of k for an arbitrary Doppler gate, and the ambiguity number K is defined as k_2-k_1+1.

A demonstration of the ambiguity number in a five-channel SAR system is shown in Fig. 2. It can be seen that the index of ambiguity is different along Doppler frequency, such as, $k=-1,0,1,2$ in the pink frequency block, $k=-2,-1,0,1,2$ in the blue frequency block and $k=-2,-1,0,1$ in the gold frequency block. In MUSIC methods, the ambiguity number is required to be smaller than M to ensure existence of at least one separate noise eigenvector. Therefore, only the Doppler gates in pink and gold blocks can be used to estimate PI errors.

By replacing $U(\tau,f+k\cdot f_{prf})$ by $U_k(\tau,f)$ and combining the data received by different channels, (3) can be expressed in matrix form as

$$\mathbf{S}_0(\tau,f)=\mathbf{\Gamma H}(f)\,\mathbf{U}(\tau,f)+\mathbf{N}_0(\tau,f) \tag{4}$$

where $\mathbf{S}_0(\tau,f)$ is the spectrum vector of the multi-channel SAR data, $\mathbf{\Gamma}$ is the PI error matrix, $\mathbf{H}(f)$ is the transfer matrix, $\mathbf{U}(\tau,f)$ is the spectrum vector of the strip-map single-channel SAR data and $\mathbf{N}_0(\tau,f)$ represents noise, given as

$$\mathbf{S}_0(\tau,f)=\left[S^{(1)}(\tau,f),S^{(2)}(\tau,f),\cdots,S^{(M)}(\tau,f)\right]^T \tag{5}$$

$$\mathbf{\Gamma}=diag\left\{\mathrm{e}^{j\delta_1},\mathrm{e}^{j\delta_2},\cdots,\mathrm{e}^{j\delta_M}\right\} \tag{6}$$

$$\mathbf{H}(f)=\left[\mathbf{h}_{k_1}(f),\mathbf{h}_{k_1+1}(f),\cdots,\mathbf{h}_{k_2}(f)\right] \tag{7}$$

$$\mathbf{h_k}(f)=\left[e^{j2\pi(f+kf_{prf})\Delta t_1},\cdots,e^{j2\pi(f+kf_{prf})\Delta t_M}\right]^T \tag{8}$$

$$\mathbf{U}(\tau,f)=\left[U_{k_1}(\tau,f),U_{k_1+1}(\tau,f),\cdots,U_{k_2}(\tau,f)\right]^T \tag{9}$$

Notice that $\mathbf{H}(f)$ is dependent of Doppler frequency and this will bring high computation load when averaging the estimators of PI errors along the Doppler gates. In order to tackle this problem, $\mathbf{H}(f)$ can be decomposed as

$$\mathbf{H}(f)=\mathbf{P}(f)\,\tilde{\mathbf{H}} \tag{10}$$

in which

$$\mathbf{P}(f)=diag\left\{e^{j2\pi f\Delta t_1},e^{j2\pi f\Delta t_2},\cdots,e^{j2\pi f\Delta t_M}\right\} \tag{11}$$

$$\tilde{\mathbf{H}} = [\mathbf{h_{k_1}}, \mathbf{h_{k_1+1}}, \cdots, \mathbf{h_{k_2}}] \tag{12}$$

$$\mathbf{h} = \left[e^{j2\pi \cdot kf_{prf}\Delta t_1}, \cdots, e^{j2\pi \cdot kf_{prf}\Delta t_M}\right]^T \tag{13}$$

By multiplying by the conjugate of $\mathbf{P}(f)$, $\mathbf{H}(f)$ can be made independent with Doppler frequency [15] and (4) is transformed to:

$$\begin{aligned}&\mathbf{S}(\tau, f) = \mathbf{P}^*(f)\mathbf{S}_0(\tau, f)\\ &=\mathbf{P}^*(f)\mathbf{\Gamma H}(f)\mathbf{U}(\tau, f) + \mathbf{P}^*(f)\mathbf{N}_0(\tau, f)\\ &= \mathbf{\Gamma}\tilde{\mathbf{H}}\mathbf{U}(\tau, f) + \mathbf{N}\end{aligned} \tag{14}$$

where $[\bullet]^*$ represents the conjugate operation. Usually, the covariance matrix of multi-channel SAR can be estimated from the sample covariance matrix $\widehat{\mathbf{R}}$, which is the statistical average along the range dimension. Here, since the steering vector $\tilde{\mathbf{H}}$ is independent of Doppler frequency, $\widehat{\mathbf{R}}$ can then be estimated along both range dimension and Doppler dimension [15]. As a result, the computational load will be significantly reduced and the SNR will increase, which is beneficial to the estimation of PI errors. For simplicity, the variables τ and f are hidden in the following derivation.

III. Rotational Invariance Property

According to the definition of equivalent time delay in (2), an arbitrary column of matrix $\tilde{\mathbf{H}}$, namely the steering vector in the field of array signal processing, is a geometric progression. Therefore, $\tilde{\mathbf{H}}$ is a Vandermonde matrix. In order to facilitate the subsequent analysis, the geometric proportions of steering vectors in all columns, called rotation matrix, are written as

$$\mathbf{D} = diag\left\{e^{j2\pi k_1 \cdot f_{prf}\Delta t}, \cdots, e^{j2\pi k_2 \cdot f_{prf}\Delta t}\right\} \tag{15}$$

Extracting the first $(M-1)$ rows and the last $(M-1)$ rows of multi-channel SAR signal in (14) and ignoring the PI errors temporarily, two equations can be built as

$$\mathbf{S}_1 = \mathbf{H}_1\mathbf{U} + \mathbf{N}_1 \tag{16}$$

$$\mathbf{S}_2 = \mathbf{H}_2\mathbf{U} + \mathbf{N}_2 \tag{17}$$

According to the definition, $\mathbf{H}_2 = \mathbf{H}_1\mathbf{D}$. Combine (16) and (17) into a matrix as

$$\overline{\mathbf{S}} = \begin{bmatrix}\mathbf{S}_1\\ \mathbf{S}_2\end{bmatrix} = \begin{bmatrix}\mathbf{H}_1\\ \mathbf{H}_1\mathbf{D}\end{bmatrix}\mathbf{U} + \begin{bmatrix}\mathbf{N}_1\\ \mathbf{N}_2\end{bmatrix} = \overline{\mathbf{H}}\mathbf{U} + \overline{\mathbf{N}}. \tag{18}$$

The corresponding covariance matrix is give by

$$\mathbf{R} = \underset{\tau,f}{E}\left[\overline{\mathbf{S}}\overline{\mathbf{S}}^{\mathrm{H}}\right] = \overline{\mathbf{H}}\underset{\tau,f}{E}\left[\mathbf{U}\mathbf{U}^{\mathrm{H}}\right]\overline{\mathbf{H}}^{\mathrm{H}} + \mathbf{R}_{\mathrm{N}} \tag{19}$$

where $[\bullet]^{\mathrm{H}}$ represents the conjugate-transpose operation, $E[\bullet]$ is expectation and $\mathbf{R}_{\mathrm{N}}$ is the noise covariance matrix. With eigen-decomposition, $\mathbf{R}$ can be decomposed as $\mathbf{R} = \mathbf{G}\cdot\mathbf{\Lambda}\cdot\mathbf{G}^{\mathrm{H}}$, where $\mathbf{\Lambda}$ and $\mathbf{G}$ are the eigenvalues and corresponding eigenvectors, respectively. Based on the spectral analysis theory, we can obtain the signal subspace $\mathbf{G}_{\mathrm{s}}$ and noise subspace $\mathbf{G}_{\mathrm{n}}$ and $\mathbf{G}_{\mathrm{s}}$ is the same as that spanned by $\overline{\mathbf{H}}$ [14]. Then there exists a unique non-singular matrix $\mathbf{T}$ that satisfies

$$\mathbf{G}_{\mathrm{s}} = \overline{\mathbf{H}}\mathbf{T} \tag{20}$$

and $\mathbf{G}_{\mathrm{s}}$ can be decomposed into

$$\mathbf{G}_{\mathrm{s}} = \begin{bmatrix}\mathbf{G}_1\\ \mathbf{G}_2\end{bmatrix} = \begin{bmatrix}\mathbf{H}_1\\ \mathbf{H}_1\mathbf{D}\end{bmatrix}\mathbf{T} \tag{21}$$

where $\mathbf{G}_1$ and $\mathbf{G}_2$ are the signal eigenvectors corresponding to the first $(M-1)$ channels sub-array and the last $(M-1)$ channels sub-array, respectively. Then, we have

$$\mathbf{G}_2 = \mathbf{H}_1\mathbf{D}\mathbf{T} = \mathbf{G}_1\mathbf{T}^{-1}\mathbf{D}\mathbf{T} = \mathbf{G}_1\mathbf{\Phi} \tag{22}$$

where $\mathbf{\Phi} = \mathbf{T}^{-1}\mathbf{D}\mathbf{T}$. In the area of direction of arrival (DOA) estimation, the rotation matrix $\mathbf{D}$ is unknown, and it can be obtained once the matrix $\mathbf{\Phi}$ is solved as

$$\mathbf{\Phi} = \mathbf{G}_1^{+}\mathbf{G}_2 \tag{23}$$

in which $[\bullet]^{+}$ denotes the pseudoinverse. By contrast, the rotation matrix $\mathbf{D}$ is known in the SAR system. Therefore, the diagonal matrix consisting of the eigenvalues of $\mathbf{\Phi}$ should be the same as the rotation matrix $\mathbf{D}$, ie.,

$$\lambda\{\mathbf{\Phi}\} = \mathbf{D} \tag{24}$$

Since the derivation above is similar with ESPRIT, this property is named as the 'rotational invariance property' for multi-channel SAR, which essentially indicates the inherent distribution property of equivalent phase centers. It is necessary to point out that the restriction on ambiguity number *K* can be relaxed. In the terms of DOA estimation, the array element number (channel number *M* in our work) should be larger than signal source number (ambiguity number *K* in our work) to make sure that all DOAs can be found. However, this is not an issue in multi-channel SAR. If $M < K$, then only $(M-1)$ elements in rotation matrix $\mathbf{D}$ correspond to the eigenvalues of $\mathbf{\Phi}$. An an extreme case, assuming $M = 2$ or only using two channels' data to estimate, $\mathbf{\Phi}$ will collapse to a complex number ϕ, which is equal to the steering element d corresponding the maximum spectrum power out of $\mathbf{D}$ as

$$\phi = d = e^{j2\pi(0)\cdot f_{prf}\Delta t} = 1 \tag{25}$$

From the aspect of ambiguities, the 3dB criteria, which is commonly used to discriminate the signal with ambiguities, is not definitely required. Reference [12] provides another definition of effective bandwidth to separate signal and ambiguities. In the extreme, effective bandwidth can be set as the PRF, and then the ambiguity number will become one, which means two channels' data can exhibit the 'rotational invariance property'.

IV. Estimation Method

A. Estimation method of PI errors

Section III shows that the rotational invariance property is based on the Vandermonde matrix $\mathbf{H}$. However, this property will not hold when PI errors $\mathbf{\Gamma}$ exist. As a result, the eigenvalues of $\mathbf{\Phi}$ calculated by (23) will not be the same as the rotation matrix $\mathbf{D}$. To illustrate this effect, a set of six-channel experimental data collected in a SAR ground test are analyzed. The parameters are listed in Table I. Fig. 3 shows the distribution of eigenvalues of $\mathbf{\Phi}$ and $\mathbf{D}$ with PI errors between channels in the complex plane. It can be seen that eigenvalues of $\mathbf{D}$ are uniformly distributed on the unit circle whereas those of $\mathbf{\Phi}$ are spread around the unit circle.

Naturally, the PI errors can be determined by the distortion of eigenvalues of $\mathbf{\Phi}$. To estimate PI errors between channels,

TABLE I: Parameters of the SAR ground test equipment.

Antenna length	Slant range	Velocity	PRF	Wavelength
1.5m x 6	770km	7236m/s	1500Hz	0.03m

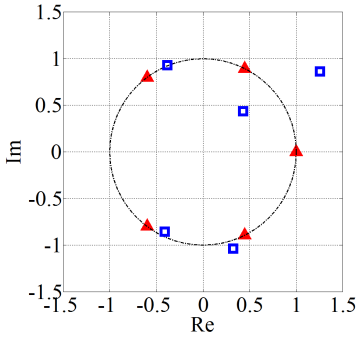

Fig. 3: Distribution of eigenvalues of $\mathbf{D}$ and $\mathbf{\Phi}$ with red '△' and blue '□', respectively, in the complex plane.

the minimum eigenvalue distance between $\mathbf{\Phi}$ and $\mathbf{D}$ is adopted in this work. The optimization problem can be formulated as

$$\hat{\mathbf{\Gamma}} = \arg\min_{\mathbf{\Gamma}} \|\mathbf{D} - \lambda(\mathbf{\Phi})\|_2 \tag{26}$$

in which $\|\bullet\|_2$ denotes the l_2 norm.

B. The quick estimation strategy

In practice, there exists cross-interference between the eigenvalues in the optimization process, which lead to a wrong convergence point. To solve this problem, an efficient alternative method is to deal with two adjacent channels of data at a time. Considering the effect of PI error between adjacent channels, (25) becames

$$\phi_m = e^{j(\delta_m - \delta_{m-1})} d = e^{j(\delta_m - \delta_{m-1})} \tag{27}$$

where the subscript '*m*' represents the estimated ϕ in the *m*-th channel. Then, δ_m can be calculated as

$$\delta_m = \delta_{m-1} + \angle\phi_m \tag{28}$$

where $\delta_1 = 0$ and $\angle(\bullet)$ denotes the phase-extraction operator. By using the quick estimation strategy, the interference between channels can be removed and higher estimation efficiency can be achieved than the optimization approach.

The flowchart of the proposed estimation method is shown in Fig. 4. By applying the FFT, the multi-channel SAR signals are transformed into the Doppler domain. After compensating the conjugate of $\mathbf{P}(f)$, the signals of adjacent channels can be used to construct the covariance matrix $\mathbf{R}$. With eigen-decomposition, the signal subspace $\mathbf{G}_s$ can then be estimated, which is a combination of $\mathbf{G}_1$ and $\mathbf{G}_2$. Finally, ϕ_m can be calculated by (23) and PI error δ_m is calculated by (28).

C. Estimation of Doppler centroid

In the multi-channel SAR, it is difficult to estimate the Doppler centroid using conventional methods due to the undersampling. Considering the effect on the matrix $\mathbf{\Phi}$, the Doppler centroid will introduce a spectrum shift on each of its eigenvalues. If the Doppler centroid is not exact, the error will result in a residual Doppler centroid term in (27) as

$$\bar{\phi}_m = e^{j(\delta_m - \delta_{m-1} + 2\pi\cdot\Delta f_d \Delta t)} \tag{29}$$

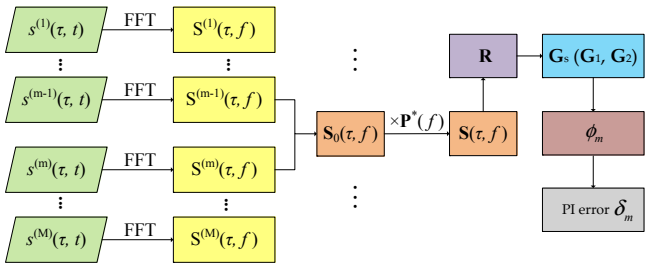

Fig. 4: The flowchart of proposed estimation method.

TABLE II: Experimental results of PI errors.

Channel	1	2	3	4	5	6
PI error (°)	0	40	-30	18	35	-5
Proposed method (°)	0	40.35	-29.58	18.86	35.44	-4.53
IOS method (°)	0	42.02	-28.39	17.72	33.39	-5.99
AWLS method (°)	0	44.10	-30.43	10.78	21.50	-10.6

To remove the added Doppler centroid term, another group of virtual adjacent channels, consisting of the *M*-th channel in the first pulse and the first channel in the following pulse, are also employed to estimate ϕ. Using $\bar{\phi}_1$ to represent the estimated result, we have

$$\bar{\phi}_1 = e^{j(\delta_1 - \delta_M + 2\pi\cdot\Delta f_d \Delta t^{\mathrm{P}})} \tag{30}$$

where $\Delta t^{\mathrm{P}} = v/f_{prf} - (M-1)\Delta t$. Then the PI errors can be cancelled out by the product of $\bar{\phi}_m$ and Doppler centroid error can be obtained as

$$\Delta f_d = \angle\left(\prod \bar{\phi}_m\right) \Big/ (2\pi \cdot v/f_{prf}) \tag{31}$$

After compensating for the residual Doppler centroid in (31), the PI errors can then be estimated by (28).

V. Experimental Results

To demonstrate the performance of the proposed method, experiments with both simulated and real data are carried out.

A. Simulated Data

The parameters listed in Table I are used to simulate a set of spaceborne multi-channel SAR data. The added PI errors and corresponding results estimated by the proposed method in comparison with improved OS method (IOS) [15] and AWLS method are shown in Table II. It is obvious that the proposed method has better estimation results. To further demonstrate its performance, Monte Carlo simulations with 100 runs are conducted. The PI errors are set randomly between $\pm 40°$ and the average root-mean-square error (ARMSE) [6] is used to quantize the estimation performance versus SNR and sampling uniformity F_u, which is defined as the ratio of operating PRF to PRF in case of uniform sampling [11].

From the results in Fig. 5 (a), the proposed method (called ESPRIT method) can achieve better estimation results against SNR than the other two methods. ESPRIT method is also more robust against F_u than its competitors, especially in the case of high non-uniformity (see Fig. 5 (b)). When the PRF is low (F_u = 0.9), there are not enough Doppler bins for the other two methods. In the case of coinciding sampling (F_u = 1.2), the noise, especially at the edge segments of bandwidth, will

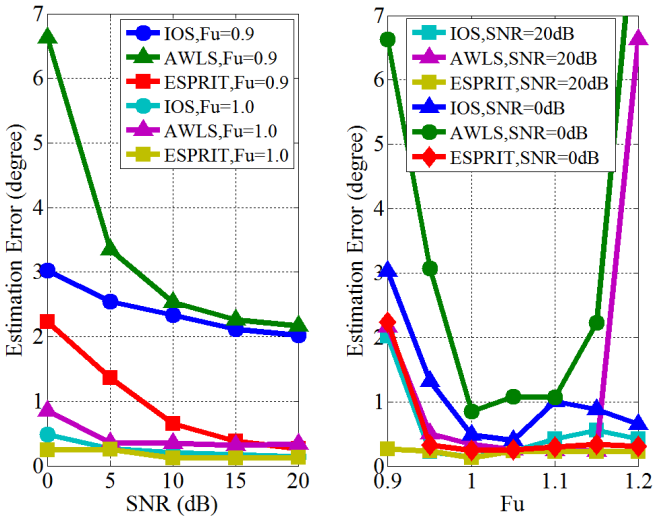

(a) (b)

Fig. 5: PI error estimation precisions of IOS method, AWLS method and proposed method versus SNR (a) and Fu (b).

TABLE III: Parameters of the Airborne SAR System.

Antenna length	Slant range	Velocity	PRF	Wavelength
0.16m x 4	12km	120m/s	380Hz	0.05m

be significantly amplified by the reconstruction filter, which will significantly effects the performance of AWLS.

As for the computational load, the proposed method shares a similar complexity with the IOS method on $O(M^3)$ [15] since they both adopt the Doppler-independent $\mathbf{H}$ in the procedures while the computational complexity of AWLS method is $N_a \cdot O(M^3)$ where N_a is the number of Doppler bins used. Note that a Doppler centroid error (100 Hz) was added for the proposed ESPRIT method in this experiment to show its ability to estimate and remove the Doppler centroid error.

B. Real Data

Real airborne SAR data are used here to show the effectiveness of the proposed method. The parameters of the SAR data are given in Table III. After processing the four-channel data with the chirp scaling algorithm, an image is obtained. There are serious ambiguity issues in Fig. 6 (a), since the PI error between channels is not estimated and compensated. Using the proposed method, the phase inconsistency errors are estimated as 0°, 123.2°, 29.2° and 161.0°. After phase compensation, the resultant image is focused excellently without obvious ambiguities as shown in Fig. 6 (b).

VI. Conclusion

Based on the analysis of a multi-channel SAR mode, the rotation invariance property of its steering vector was obtained. It was found that the eigenvalues of spectrum matrix of multi-channel signals are not uniformly distributed when phase errors exist. Therefore, a novel PI error estimation method, which exploits the distortion in the eigenvalue distribution, is proposed. As demonstrated by experimental results based on simulated and real data, the proposed method can estimate the Doppler centroid effectively and outperforms the conventional

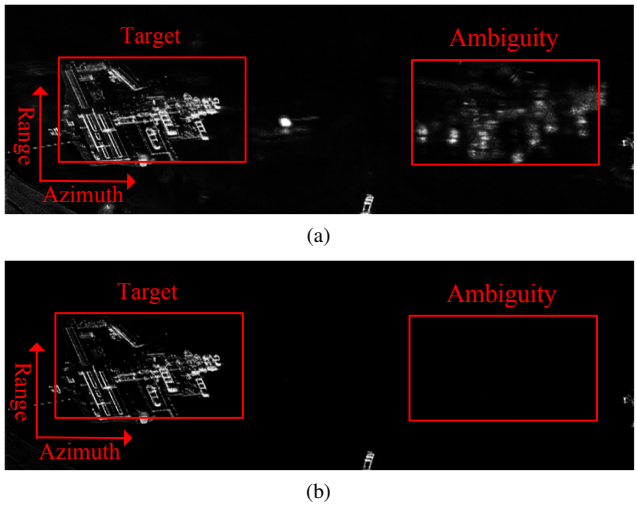

(a)

(b)

Fig. 6: Images of airborne SAR before and after PI correction.

methods, especially in the high non-uniform sampling case. It also benefits from lower computational complexity.

References

[1] G. Krieger, N. Gebert, and A. Moreira, "Unambiguous SAR signal reconstruction from nonuniform displaced phase center sampling," *IEEE Trans. Signal Process.*, vol. 1, no. 4, pp. 260–264, 2004.

[2] N. Gebert, G. Krieger, and A. Moreira, "Digital beamforming on receive: techniques and optimization strategies for high-resolution wide-swath SAR imaging," *IEEE Trans. Aerosp. Electron. Syst.*, vol. 45, no. 2, pp. 564–592, 2009.

[3] L. Brule, D. Delisle, H. Baeggli, and J. Graham, "RADARSAT-2 program update," in *Proc. IGARSS*, Seoul, Korea, Jul. 2005, p. 3.

[4] J. Janoth, S. Gantert, T. Schrage, and A. Kaptein, "Terrasar next generation - mission capabilities," in *Proc. IGARSS*, Melbourne, VIC, Australia, Jul. 2013, pp. 2297–2300.

[5] Z. Li, H. Wang, T. Su, and Z. Bao, "Generation of wide-swath and high-resolution SAR images from multichannel small spaceborne SAR systems," *IEEE Geosci. Remote Sens. Lett.*, vol. 2, no. 1, pp. 82–86, 2005.

[6] T. Yang, Z. Li, Y. Liu, and Z. Bao, "Channel error estimation methods for multichannel SAR systems in azimuth," *IEEE Geosci. Remote Sens. Lett.*, vol. 10, no. 3, pp. 548–552, 2013.

[7] J. Feng, C. Gao, Y. Zhang, and R. Wang, "Phase mismatch calibration of the multichannel SAR based on azimuth cross correlation," *IEEE Geosci. Remote Sens. Lett.*, vol. 10, no. 4, pp. 903–907, 2013.

[8] A. Liu, G. Liao, Q. Xu, and L. Ma, "An improved array-error estimation method for constellation SAR systems," *IEEE Geosci. Remote Sens. Lett.*, vol. 9, no. 1, pp. 90–94, 2012.

[9] Z. Li, Z. Bao, H. Wang, and G. Liao, "Performance improvement for constellation SAR using signal processing techniques," *IEEE Trans. Aerosp. Electron. Syst.*, vol. 42, no. 2, pp. 436–452, 2006.

[10] A. Liu, G. Liao, L. Ma, and Q. Xu, "An array error estimation method for constellation sar systems," *IEEE Geosci. Remote Sens. Lett.*, vol. 7, no. 4, pp. 731–735, 2010.

[11] Y.-Y. Liu, Z.-F. Li, T.-L. Yang, and Z. Bao, "An adaptively weighted least square estimation method of channel mismatches in phase for multichannel SAR systems in azimuth," *IEEE Geosci. Remote Sens. Lett.*, vol. 11, no. 2, pp. 439–443, 2014.

[12] B. Liu and Y. He, "Improved DBF algorithm for multichannel high-resolution wide-swath SAR," *IEEE Trans. Geosci. Remote Sens.*, vol. 54, no. 2, pp. 1209–1225, 2016.

[13] Z. Wang, Y. Liu, Z. Li, G. Xu, and J. Chen, "Phase bias estimation for multi-channel HRWS SAR based on Doppler spectrum optimization," *Electron. Lett.*, vol. 52, no. 21, pp. 1805–1807, 2016.

[14] P. Stoica and R. L. Moses, *Spectral Analysis of Signals*. NJ, USA: Pearson Prentice Hall, 2005.

[15] X. Guo, Y. Gao, K. Wang, and X. Liu, "Improved channel error calibration algorithm for azimuth multichannel SAR systems," *IEEE Geosci. Remote Sens. Lett.*, vol. 13, no. 7, pp. 1022–1026, 2016.